

# Seasonal variation in formation, structure, and chemical properties of phloem in *Picea abies* as studied by novel microtechniques

Tuula M. Jyske<sup>1</sup> · Jussi-Petteri Suuronen<sup>2,3</sup> · Andrey V. Pranovich<sup>4</sup> ·  
Tapio Laakso<sup>1</sup> · Ugai Watanabe<sup>5</sup> · Katsushi Kuroda<sup>6</sup> · Hisashi Abe<sup>6</sup>

Received: 15 January 2015 / Accepted: 5 June 2015 / Published online: 24 June 2015  
© Springer-Verlag Berlin Heidelberg 2015

## Abstract

**Main conclusion** Phloem production and structural development were interlinked with seasonal variation in the primary and secondary metabolites of phloem. Novel microtechniques provided new perspectives on understanding phloem structure and chemistry.

To gain new insights into phloem formation in Norway spruce (*Picea abies*), we monitored phloem cell production and seasonal variation in the primary and secondary metabolites of inner bark (non-structural carbohydrates and phenolic stilbene glucosides) during the 2012 growing season in southern and northern Finland. The structure of

developing phloem was visualised in 3D by synchrotron X-ray microtomography. The chemical features of developing phloem tissues isolated by laser microdissection were analysed by chemical microanalysis. Within-year phloem formation was associated with seasonal changes in non-structural carbohydrates and phenolic extractive contents of inner bark. The onset of phloem cell production occurred in early and mid-May in southern and northern Finland, respectively. The maximal rate of phloem production and formation of a tangential band of axial phloem parenchyma occurred in mid-June, when total non-structural carbohydrates peaked (due to the high amount of starch). In contrast, soluble sugar content dropped during the most active growth period and increased in late summer and winter. The 3D visualisation showed that the new axial parenchyma clearly enlarged from June to August. Sub-cellular changes appeared to be associated with accumulation of stilbene glucosides and soluble sugars in the newest phloem. Stilbene glucosides also increased in inner bark during late summer and winter. Our findings may indicate that stilbene biosynthesis in older phloem predominantly occurs after the formation of the new band(s) of axial parenchyma. The complementary use of novel microtechniques provides new perspectives on the formation, structure, and chemistry of phloem.

**Keywords** Carbohydrates · Laser microdissection · Microtomography · Phloem parenchyma · Phenolics · Stilbene glucosides

## Abbreviations

BH Breast height (1.3 m)  
CB Base of the living crown  
LMD Laser microdissection  
N1 Site at Kivalo, in northern Finland

Special topic: Polyphenols: biosynthesis and function in plants and ecosystems. Guest editor: Stefan Martens.

**Electronic supplementary material** The online version of this article (doi:10.1007/s00425-015-2347-8) contains supplementary material, which is available to authorized users.

✉ Tuula M. Jyske  
tuula.jyske@luke.fi

<sup>1</sup> Natural Resources Institute Finland (Luke), New Business Opportunities, Jokiniemenkuja 1, 01370 Vantaa, Finland

<sup>2</sup> ESRF-The European Synchrotron, CS40220, 38043 Grenoble Cedex 9, France

<sup>3</sup> Department of Physics, University of Helsinki, P.O.B 64, 00014 Helsinki, Finland

<sup>4</sup> Process Chemistry Center, Åbo Akademi University, Porthaninkatu 3, 20500 Turku, Finland

<sup>5</sup> Department of Life and Environmental Sciences, Chiba Institute of Technology, 2-17-1 Tsudanuma Narashino, Chiba 275-0016, Japan

<sup>6</sup> Forestry and Forest Products Research Institute, 1 Matsunosato, Tsukuba 305-8687, Japan

NSC	Non-structural carbohydrates (defined here as soluble sugars + starch)
S1	Site 1, Haapastensyrjä, in southern Finland
S2	Site 2, Ruotsinkylä, in southern Finland
μCT	Synchrotron X-ray microtomography

## Introduction

Norway spruce [*Picea abies* (L.) Karst.] phloem (i.e. inner bark) consists of sieve cells associated with albuminous cells and of axial and ray parenchyma (Franceschi et al. 1998, 2005; Evert 2006). The size and number of functional sieve cells determine the conductive capacity of phloem, whereas ray parenchyma allows the exchange of water and assimilates to occur between phloem and xylem through lateral translocation (van Bel 1990; Froelich et al. 2011; Spicer 2014; Jyske and Hölttä 2015). Phloem parenchyma also serves as a storage tissue and contains marked reserves of starch and lipids (Franceschi et al. 1998; Krekling et al. 2000). In addition, the network of axial and ray parenchyma is an essential constituent of the multi-tiered defence system of Norway spruce. This system includes both constitutive and inducible protective mechanisms against invasive organisms, such as bark-beetles and pathogenic fungi (e.g. Franceschi et al. 1998, 2000, 2005; Nagy et al. 2000, 2014; Krokene et al. 2008; Hammerbacher et al. 2011).

Axial phloem parenchyma seems to be the main site of phenolic metabolite accumulation; therefore, it is also called polyphenolic parenchyma (Franceschi et al. 1998, 2005; Krokene et al. 2008; Li et al. 2012). Among the most abundant phenolic secondary metabolites in Norway spruce phloem are stilbene glucosides and their aglycons (e.g. Latva-Mäenpää et al. 2013, 2014; Jyske et al. 2014b). The hydroxylated stilbene glucosides *trans*-astringin and *trans*-isorhapontin are the major stilbene compounds, while the trihydroxystilbene *trans*-piceid is a minor one (e.g. Latva-Mäenpää et al. 2013). These antioxidant stilbenoids likely provide protection against a variety of environmental stressors (Franceschi et al. 2005; Witzell and Martin 2008; Chong et al. 2009). Due to their antifungal and antimicrobial properties, stilbene compounds may also contribute to human health or material science (e.g. Manach et al. 2004; Rossi et al. 2013; Robb and Stuart 2014). Spruce bark, which is rich in stilbenes, could be utilised as a raw material in biorefinery activities, and is readily available as large amounts of spruce bark-waste are produced each year in forestry.

The growing economic interest in spruce bark stilbenes requires a deeper understanding of their variation within and between trees and accumulation patterns within bark tissues (Krogell et al. 2012; Jyske et al. 2014b). However,

the mechanisms of formation, accumulation, and metabolism of stilbene derivatives in planta are still far from being understood (Chong et al. 2009). Stilbene glucosides, for example, are found in all layers of spruce secondary phloem, but their quantities and relative proportions differ between young (inner) and older (outer) layers (Jyske et al. 2014b). There is also some evidence of seasonal variation in stilbene glucoside content (Solhaug 1990). Indeed, seasonal changes in the amounts of contents stored in vacuoles in axial phloem parenchyma have been recorded: both storage starch granules and phenolic bodies differed depending on the time of year (Krekling et al. 2000). However, little is known about the seasonal regulation of stilbene synthesis and accumulation during a growing season.

A significant amount of photo-assimilated carbon may be used in the synthesis of constitutive (and inducible) secondary metabolites. Carbon is also required for the construction of new secondary phloem and xylem and to maintain the metabolism for construction and maintenance of living tissues. Thus, a trade-off may exist in the allocation of carbon between growth and defence at the whole-organism level, as suggested by the growth-differentiation balance hypotheses (Herms and Mattson 2012). However, the sink–source relations may differ between tissues.

New photoassimilates are transported by phloem from the source leaves to sinks and used there as substrates (Kozłowski 1992). Non-structural carbohydrate (NSC) pools are commonly presumed to serve as substrates, in order to alleviate the temporal imbalances between photoassimilate production and high sink demand (Kozłowski 1992). A number of studies have associated the within-year dynamics of NSCs in xylem and cambium with xylem increment growth (e.g. Sundberg et al. 1993; Deslauriers et al. 2009, 2014; Giovannelli et al. 2011; Gruber et al. 2013; Simard et al. 2013), whereas fewer studies have elucidated the seasonal patterns of phloem NSCs (Antonova and Stasova 2006, 2008; Gruber et al. 2013). In addition, few studies have examined the association between within-year phloem production quantities and/or accumulation of primary and secondary (constitutive) metabolites (cf. Solhaug 1990; Krekling et al. 2000; Antonova and Stasova 2008). In general, our knowledge of the seasonal processes of phloem formation in Norway spruce is limited (e.g. Gričar et al. 2014), partly owing to the difficulties of observing fragile phloem structures, which often require time-consuming specimen preparation for electron microscopy or use of new imaging techniques (van Bel 2003; Spicer 2014; Truernit 2014).

In the present study, we aimed to elucidate the processes and control of phloem formation, with special emphasis on axial phloem parenchyma and secondary phenolic stilbene compounds. This study is the first attempt to understand the temporal and spatial patterns of phloem stilbene

accumulation and its relationship to phloem tissue growth and within-year variation in primary metabolites. We examined the relationships between the within-year development of phloem structural and chemical properties in mature Norway spruce growing in boreal region in northern and southern Finland. In particular, we examined the seasonal changes in (1) phloem cell production, (2) NSCs, and (3) stilbene glucoside content of inner bark (i.e. all the tissues from cambium up to the innermost periderm; Trockenbrodt 1990). In addition, we analysed phloem cellular and sub-cellular structures in 3D by synchrotron X-ray microtomography ( $\mu$ CT) and conducted quantitative chemical microanalysis of developing phloem isolated by laser microdissection (LMD). Our hypotheses were that (1) the amount of NSC in inner bark would show seasonal variation reflecting the demands of phloem formation and secondary metabolite accumulation; (2) secondary metabolite accumulation would take place in newly developed phloem during the course of the growing season, and (3) the changes in the chemical properties of developing phloem would be interlinked with the developmental changes in the contents of axial phloem parenchyma cells.

## Materials and methods

### Study sites and sample trees

The study was conducted on dominant and co-dominant Norway spruce (*Picea abies* (L.) Karst.) trees growing at two sites in southern Finland (S1: Haapastensyrjä tree breeding centre, 60°4'N, 24°3'E, 120 m above sea level (a.s.l.); S2: Ruotsinkylä research forest, 60°2'N, 25°0'E, 60 m a.s.l.) and one site in northern Finland (N1: Kivalo research forest, 66°2'N, 26°4'E, 140 m a.s.l.). The trees in S1 were rooted cuttings originating in southern Finland (clone no. 255; Jyske et al. 2014b; Jyske and Hölttä 2015). The cuttings were planted on a fertile stand of old agricultural land. In S2 and

N1, the selected trees were grown from local seeds and were planted on the fertile soil where Norway spruces typically grow. The trees were 30, 41, and 69 years old at S1, S2, and N1, respectively. Four (S2 and N1) or three (S1) trees of similar size were selected in each site. Samples were collected from breast height (BH) (about 1.3 m), where the average diameter was 22 cm. In addition, at S1, samples for phloem tomography were obtained at the base of the living crown (CB, 13 m; Table 1).

### Monitoring phloem and xylem formation

We monitored phloem and xylem formation weekly during the 2012 growing season. We extracted small microcores (diameter 2 mm, length 15 mm; Rossi et al. 2006a) at BH at each site as described in Jyske et al. (2014a). The microcores were preserved in 50 % ethanol at 4 °C. The microcores were dehydrated in a graded series of ethanol and ethanol–resin mixture (LR White Resin, medium grade, London Resin Co., Ltd., London, UK). The specimens were embedded into resin blocks and transverse sections (ca. 5–8  $\mu$ m thick) were cut with a rotary microtome (Leica RM2265, Leica Microsystems, Wetzlar, Germany) using glass knives. The sections were stained with an aqueous solution of cresyl violet acetate (Sigma-Aldrich, Saint-Louis, MO, USA), air dried, and permanently mounted on objective slides using Ultrakitt M540 mountant (TAAB, Reading, UK).

Images of the developing annual rings of xylem and phloem were taken using a digital camera (MicroPublisher 3.3 RTV, QImaging, Surrey, Canada) attached to a light microscope (Olympus BX60, Olympus, Tokyo, Japan) at 10 $\times$  magnification (resolution 0.234  $\mu$ m pixel<sup>-1</sup>). One image was used or several overlapping images were joined to cover the whole width of the current-year tissues. In the current xylem growth ring, the number of tracheids was counted, and in the phloem growth ring, the numbers of sieve cells and axial parenchyma cells in a radial file were

**Table 1** Sampling day of the year (DOY), and the corresponding date, for the analysis of non-structural carbohydrates and stilbene glucosides of inner bark in samples from three sites (S1, Haapastensyrjä; S2, Ruotsinkylä; N1, Kivalo)

Period	Dates			
	S1	S2	N1	
1	76	16-March-2012	86	26-March-2012
2	117	26-April-2012	128	07-May-2012
3	145 <sup>μ</sup>	24-May-2012	144	06-June-2012
4	172 <sup>*μ</sup>	20-June-2012	174	02-July-2012
5	208 <sup>*</sup>	26-July-2012	208	nd
6	243 <sup>*μ</sup>	30-August-2012	243	03-September-2012
7	292	18-October-2012	289	15-October-2012
8	10	10-January-2013	9	08-January-2013

\* Laser microdissection and chemical microanalysis of developing phloem in S1

<sup>μ</sup>  $\mu$ CT of developing phloem at S1 and N1, nd not detected

determined. Sieve cells and axial parenchyma were distinguished on the basis of their morphology and cell contents. For example, starch and extractives tended to be present in axial parenchyma, which also displayed a more rounded cell form than sieve cells (see Jyske and Hölttä 2015). Cambial cells were identified on the basis of their smaller radial diameter and thinner primary walls, compared with phloem and xylem cells.

Phloem and xylem cell production were defined to have begun when at least one new phloem and xylem cell in the enlargement phase, respectively, was observed after cambial reactivation. Xylem and phloem cell incitement was modelled by applying the Gompertz-function to the cell counts (e.g. Zeide 1993; Rossi et al. 2003). Phloem usually contained one to two overwintering sieve cells next to non-dividing cambium at the time of the first microcore sampling. To ease Gompertz fitting, these cells were omitted from the phloem cell counts throughout the growing season. Only the phloem and xylem derivatives produced by cell divisions after the cambial reactivation in spring were included in the analysis. For each site, we calculated the day of the year (DOY) when 5, 50, and 90 % of the total number of phloem or xylem cells had been produced and the DOY when the rate of maximal cell production occurred (cells day<sup>-1</sup>; for details, see Jyske et al. 2014a). In addition, the mean DOY of formation of the first tangential band of axial parenchyma was computed for each site. This date also represented the onset of late phloem formation.

### Sampling and specimen preparation for chemical analysis of inner bark

To study the connections between within-year phloem formation and the NSC and stilbene glucoside content of inner bark, we collected small intact blocks of wood (ca. 2 cm tangential × 5 cm longitudinal × 2 cm radial, respectively) once a month at BH from two trunks at each site (Table 1). The sample blocks were immediately frozen, transported to the laboratory in dry ice (−78 °C), and stored at −78 °C until further processing. Rhytidome was scraped away with a razor blade. Inner bark (including cambium, all the tissues from cambium to the innermost periderm, and possibly some remaining developing xylem) was separated from xylem on the basis of the hardness and colour differences between the tissues. The sample blocks were divided into two or three sub-samples, which were used for carbohydrate and stilbene analysis and LMD (Table 1).

### Non-structural carbohydrates (NSC) analysis of inner bark

NSCs (i.e. soluble sugars + starch) were analysed using a single sub-sample. Samples were cut into matchstick-sized

pieces, freeze-dried for 72 h, and milled with a ball-mill while still frozen. About 50 mg of powder was weighed into glass test tubes and heated to 100 °C to deactivate the enzymes. The soluble sugars were extracted from the samples in a water bath (100 °C) containing 80 % ethanol to which m-erythrit (Calbiochem, Merck KGaA, Darmstadt, Germany) was added as an internal standard. The sugar extracts were evaporated to dryness with nitrogen flow, silylated with 20 % TMSI-pyridine mixture (1-trimethylsilyl-imidazole; Sigma-Aldrich), and analysed with gas chromatography–mass spectrometry (GC–MS; Agilent Hewlett-Packard 6890 GC, equipped with a Zebron ZB-SemiVolatiles column (30 m × 0.25 mm i.d. × 0.25 µm df) and Hewlett-Packard 5973 MSD, EI-MS 70 eV), in which helium was used as a carrier gas (flow 1.5 ml/min). The chromatographic conditions were as follows: initial temperature 110 °C; rate of temperature increase 10 °C min<sup>-1</sup>; final temperature 320 °C maintained for 14 min; injector temperature 260 °C, and split ratio 1:20. The MS-interface temperature was 300 °C and ion source temperature was 230 °C. The results were calculated using an internal standard and the following external standards: D-fructose (Merck), myo-inositol (Merck), D-glucose (BDH AnalaR, VWR International Ltd., Poole, UK), sorbitol (Fluka, Sigma-Aldrich), sucrose (BDH AnalaR), D-raffinose pentahydrate (Fluka). For pinitol, fructose was used as a standard, and for stachyose, raffinose was used as a standard.

The soluble sugar-free samples obtained after the extractions were used for starch analyses with a commercial starch assay kit (Total Starch Assay Procedure, Megazyme International, Wicklow, Ireland). Briefly, starch in residual pellets was hydrolysed into maltodextrins by adding α-amylase (in MOPS-buffer, pH 7) and incubating for 6 min at 100.5 °C. Next, the samples were suspended in acetate buffer (pH 4.5) and amyloglucosidase was added to hydrolyse maltodextrins into D-glucose by incubating for 30 min at 50.5 °C. The absorbance of the samples was measured colourimetrically (Shimadzu UV-2401 spectrometer at 510 nm) using glucose oxidase and peroxidase. The standard curve was made with D-glucose (BDH AnalaR).

### Stilbene glucoside analysis of inner bark

Another sub-sample was used to analyse stilbene glucoside amounts in inner bark, as described by Jyske et al. (2014b). Samples were milled into powder with an analytical mill (Kinematica, Littau/Luzern, Switzerland) equipped with a cooling unit (−30 °C), sealed in plastic vials, and stored at −78 °C in darkness. Approximately 30 mg of powder was placed in a test tube and extracted with an acetone–water solution (95:5, v/v, including 0.2 mg ml<sup>-1</sup> of

heptadecanoic acid as internal standard) in an ultrasonic water bath (USC300TH, VWR, Radnor, PA, USA) for 30 min. After sonication, the tubes were centrifuged at 1099g for 5 min, and 1 ml of supernatant of each sample was pipetted into an autosampler vial. The samples were dried with N<sub>2</sub> silylated with 0.5 ml of *N*-trimethylsilyl imidazole (TMSi in pyridine, Sigma-Aldrich) and kept in a heater at +60 °C for 30 min or at room temperature overnight before analysis.

Silylated extracts were analysed by GC–MS (Agilent Hewlett-Packard 6890 and Hewlett-Packard 5973 MSD, EI-MS 70 eV; Agilent, Santa Clara, CA, USA) equipped with a Zebtron ZB-SemiVolatiles capillary column, as described in Jyske et al. (2014b). Quantitative analysis of identified compounds (stilbene glucosides *trans*-astringin, -isorhaponin, and -piceid) was done by using an internal standard (heptadecanoic acid, C:17) and the relative response factor was determined by using stilbene glucoside *trans*-piceid (polydatin; Sigma-Aldrich, see Jyske et al. 2014b).

### Laser microdissection (LMD) of current-year phloem

We performed chemical microanalysis of developing (i.e. current-year) phloem tissues, which we isolated using LMD. Three sub-samples from S1 were selected (Table 1) to represent the most active phase, early phloem cell production (June); late phloem production (July); and the end of phloem cell production (August). From the frozen sub-blocks, serial transverse cryo-sections (100 µm thick) were cut with a rotating cryo-microtome (Microm HM505 E, Thermo Fischer Scientific, Inc., Waltham, MA, USA) at –20 °C. The cryo-sections were placed between two objective glasses and freeze-dried for 24 h (Eyela FD-1000, Tokyo Rikakikai Co., LT, Tokyo, Japan), after which they were mounted on single LMD frame slides using adhesive tape. The LMD procedure was carried out using a Leica LMD7000 (Leica Microsystems) attached to the microscope (Leica DM6000 B). Optimal dissection at 20× magnification was conducted using a laser energy intensity of 60, cutting speed of five, and aperture size of 25. Approximately 1 mg of the current-year phloem tissue (including the current-year phloem and some cambial cells) per sample was isolated and collected into 0.5 ml micro-centrifuge tube caps. The isolated tissues were visually distinguished from the older phloem tissues and developing xylem on the basis of morphology and phloem ring border (the sieve cells of the late phloem from the previous year were flattened compared with the early phloem from the current year; Fig. 1). The remaining layers of older phloem and bark after microdissection, hereafter referred to as “older phloem”, were also collected and subjected to chemical microanalysis.

### Chemical microanalysis of laser-microdissected phloem

We used the LMD-isolated tissues of developing phloem to study mono- and disaccharides, extractives, and remaining non-cellulosic polysaccharides by chemical microanalysis methods (GC and GC–MS). The LMD-isolated phloem was freeze-dried and extracted in test tubes three times with 3 ml of acetone:water (9:1, v/v) at room temperature in the dark (over a period of 24 h). Tubes were periodically agitated by hands. The clear extracts were transferred to another test tube with Pasteur’s pipettes; solvents from cumulative extracts were evaporated in a water bath at 40 °C with N<sub>2</sub> flow and dried in a vacuum desiccator (40 °C, 1 h in darkness). The amounts of dried extractives were estimated and 10 ml of acetone was added to each test tube to obtain a stock solution of extractives. Aliquots of stock solution were placed in separate test tube, xylitol and betulinol were added as standards (100 µl of 0.1 mg/ml xylitol in methanol and 2 ml of 0.02 mg/ml of betulinol in methyl *tert*-butyl ether), and solvents were evaporated under N<sub>2</sub>.

Silylation was conducted at 70 °C for 40 min with a 4:1:1 mixture of BSTFA-TMCS-pyridine (N,O-bis(trimethylsilyl) trifluoroacetamide–trimethylchlorosilane) and the derivatised sample was left overnight. Silylated samples were then analysed by GC on the long capillary columns HP-1 and HP-5 using temperature programming, which provided a simultaneous analysis of mono-/disaccharides and extractives during a single GC run. Mono- and disaccharides were quantified against xylitol using correction factors determined by separate analysis of model mono-/disaccharides. Extractives were quantified against betulinol using no correction factor (i.e. a correction factor of 1.0).

After the extraction, the dry weight of each extracted specimen was determined by a microbalance and the sample was taken for acid methanolysis in separate test tubes. After acid methanolysis, the remaining non-cellulosic polysaccharides (i.e. hemicelluloses and pectins) were decomposed to monomeric sugar units. The contents of the test tube were neutralised with pyridine, the sorbitol and resorcinol standards were added, and solvents were evaporated with N<sub>2</sub>. The residues were dried in a vacuum desiccator at 40 °C for 40 min, silylated with hexamethyldisilazane and trimethylchlorosilane in pyridine overnight according to Sundberg et al. (1996), and analysed by GC.

### 3D microtomography of phloem

We visualised developing phloem structures and quantified changes in the contents of phloem parenchyma cells during

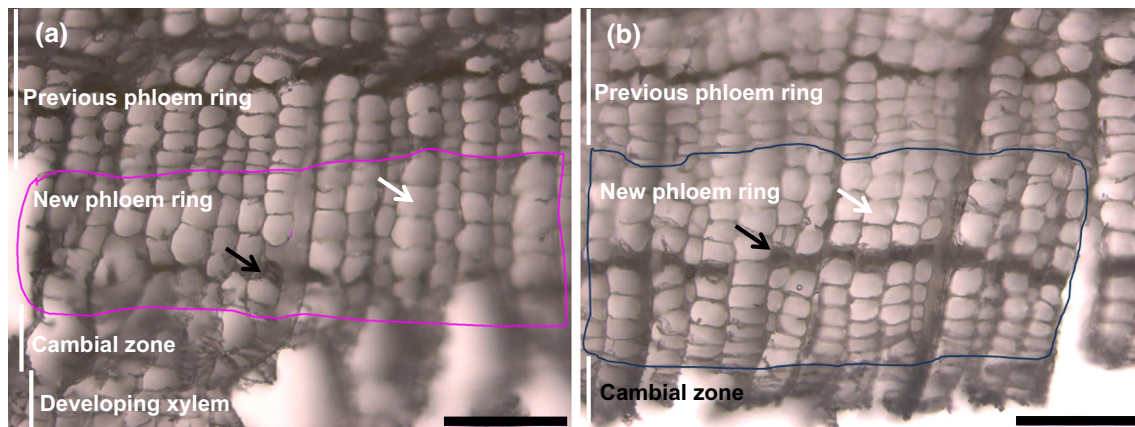


**Fig. 1** Transverse sections of Norway spruce phloem cut by a cryo-microtome and freeze-dried from samples collected in June (**a**) and August (**b**). *Purple and blue circle* indicates the area of developing

phloem to be laser microdissected. *White and black arrows* indicate sieve cells and the tangential band of axial parenchyma (i.e. polyphenolic parenchyma), respectively. *Scale bars* 100  $\mu\text{m}$

the growing season using phase-contrast synchrotron radiation X-ray microtomography ( $\mu\text{CT}$ ), which has recently gained popularity for three-dimensional analysis of xylem structure and physiology (Brodersen 2013; Cochard et al. 2015).  $\mu\text{CT}$  is a microscopic technique in which 3D voxel (volume element, cf. pixel in a 2D digital image) images of the internal structure of the sample are reconstructed, based on a series of transmission radiographs (projections) taken from different angular positions around the sample. Generally in  $\mu\text{CT}$ , high voxel values (shown in white/light grey in Figs. 3, 4 and in the supporting information) indicate material with high X-ray attenuation coefficient. When using a coherent synchrotron X-ray source, contrast in poorly attenuating materials like phloem can be enhanced by a process called phase retrieval, which links the voxel values to the phase change of the X-rays rather than attenuation. First, we collected three intact sample blocks that had similar dimensions to those used for chemical analysis, representing the times of early and late phloem production and the cessation of phloem production (Table 1). The sample blocks were fixed with a mixture of 25 % glutaraldehyde and 16 % paraformaldehyde (2:5, v/v; in 0.1 M phosphate buffer; pH 7.4). The final concentrations of glutaraldehyde and paraformaldehyde in the fixative solution were 5 and 8 % (v/v). The fixed samples were cut into  $1 \times 1 \times 5 \text{ mm}^3$  cuboids and dehydrated in a graded series of ethanol, followed by critical point drying (Leroux et al. 2009). The measurements were performed on two experimental sessions at the beamline ID19 at the European Synchrotron Radiation Facility (ESRF, Grenoble, France). Most specimens were scanned with a voxel size (edge length of one cubic voxel) of  $0.355 \mu\text{m}$ , using monochromatic 18 keV radiation and Paganin phase retrieval for enhanced contrast ( $\delta/\beta = 1500$ ). In addition, roughly half the samples were imaged

with a larger voxel size of  $0.7 \mu\text{m}$  to obtain a larger field-of-view image. The data analysis and rendering of the images was performed with Avizo (FEI, Hillsboro, OR, USA) and VGStudioMAX (Volume Graphics GmbH, Heidelberg, Germany) software.

### Statistical analysis

The amounts of NSC and stilbene glucosides were compared between the sites and sampling periods through repeated mixed model analysis (MIXED procedure, SAS 9.3 software, SAS Institute Inc., Cary, NC, USA) and with Tukey tests for multiple post hoc comparisons. The site and sampling period were considered fixed factors, and the tree was used as a random factor in the models. The sampling period within each site was assigned as a repeated-effect factor, and autoregressive covariance structure [AR(1)] was applied for the residuals. The significance of the correlations between NSC and stilbenes was tested by computing Pearson correlation coefficients ( $r$ ).

## Results

### Timing of phloem and xylem production

At the sites in southern Finland (S1 and S2), phloem cell production started in the beginning of May (Fig. 2). In northern Finland (N1), the onset of phloem cell production occurred by mid-May. Xylem cell production initiated  $\sim 3$  weeks later, in late May (S1, S2) or early June (N1). The maximal rate of phloem cell production occurred, on average, in mid-June, whereas that of xylem occurred shortly after the summer solstice. Formation of the tangential band of axial parenchyma was observed by June 10,

13, and 22 at S1, S2, and N1, respectively. At approximately the same time, half the total annual number of phloem cells had been produced (Table 2). Phloem cell production reached 90 % of its maximum level on September 28 in S1, July 27 in S2, and August 5 in N1. Meanwhile, 90 % of xylem cells had been produced

approximately 2 weeks earlier in S1 and N1 and were produced a month later in S2. At all the sites, from 10 to 15 new phloem cells were produced by cambial divisions during the growing season (11–13 cells in S1, 10–14 in S2, and 11–15 in N1; Fig. 2).

### Structural development of phloem

The  $\mu$ CT imaging of phloem clearly revealed the highly organised tissue structures in 3D (Fig. 3; Online Resource 1). Towards the outer phloem layers, secondary changes occurred that were characterised by the collapse of sieve cells and inflation of parenchyma tissue (Fig. 4). The samples representing active phloem production (collected in May at S1 and June at N1; Tables 1, 2) typically consisted of ~5 mature, non-collapsed sieve cells of the previous-year phloem ring (both early and late phloem), and several developing thin-walled phloem derivatives next to the wide cambial zone (Fig. 3a, d; Online Resource 1). At the time of late phloem formation (and early wood formation), phloem transport seemingly occurred through sieve cells from two annual rings (Fig. 3e). The sieve cells of the developing ring were separated from the previous-year ring by 1–3 flattened sieve cells of late phloem. Moving outward from the newest phloem, the shape of the axial parenchyma became more rounded, and the cellular contents increased in length and width (Fig. 4). The outer cytoplasm of older parenchyma contained many large starch granules (Fig. 4).

The new cells of axial phloem parenchyma were first observed in S1 in late May by  $\mu$ CT (Fig. 5). The newly divided cells (from samples collected in May and June at S1 and July at N1) were organised in tangential bands and appeared as elongated cells comparable in length to sieve cells, being longer than the height of the imaged region of the sample (Fig. 5a). The cell shape was rectangular and cellular deposits had a smooth appearance. The diameters of the cells were approximately half the size of those found in the previous-year axial parenchyma (Figs. 3b, 4). By June, the differentiation of axial parenchyma had continued and cells divided by transverse divisions of cells: we could clearly visualise the new developing, transverse cell walls in tangential view (Fig. 5b). By August, the newly formed, short axial parenchyma had thickened transverse walls (Fig. 5c), but few elongated cells could still be detected (Online Resource 2). This difference is illustrated also in Fig. 5d, which shows 3D renderings of the cell contents of axial parenchyma in the current and previous-year axial parenchyma in the June sample. By the end of the growing season, the cellular contents inside the axial parenchyma had noticeably increased in size, usually filling the whole cell and having a denser appearance than they had in June (S1) and July (N1) (Fig. 3b, c, e, f; Online Resource 1).

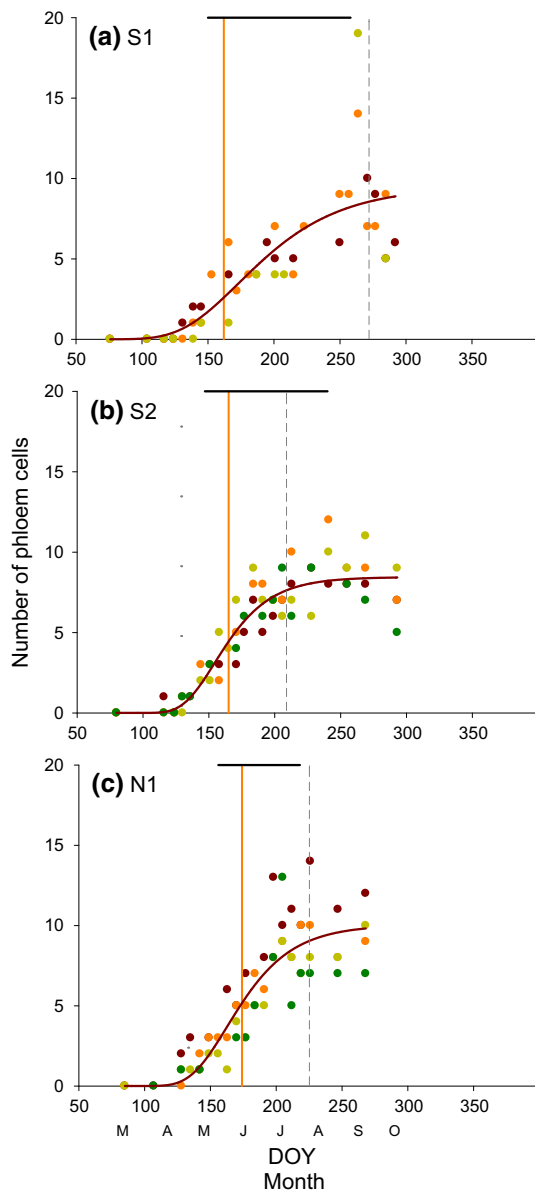


**Fig. 2** The number of phloem cells plotted against the day of the year (DOY) in southern Finland (a S1-Haapastensyrjä; b S2-Ruotsinkylä), and northern Finland (c N1-Kivalo). The dynamics of phloem formation was modelled by fitting the Gompertz-function to the data. Dots represent individual trees at each site ( $n = 3$  at S1;  $n = 4$  at S2 and N1). Vertical lines indicate the critical DOY of phloem cell production: 5 % (dotted grey), and 90 % (long grey) of the total annual number of phloem cells reached, and the time of formation of the first tangential band of axial parenchyma (orange). Horizontal black lines at top refer to the timing of xylem cell production (DOY 5–90 %)

**Table 2** Critical dates, day of the year (DOY) and the corresponding date, of phloem cell production in trees from three sites (S1, Haapastensyrjä; S2, Ruotsinkylä; N1, Kivalo) during the 2012 growing season, as predicted using the Gompertz-function (the

DOY when 5, 50, and 90 % of the total number of cells were produced), the DOY of maximal cell production rate (cells day<sup>-1</sup>), and the DOY for axial phloem parenchyma formation

Site	5 %	50 %	90 %	Maximal rate	Axial parenchyma
S1	126 (150) 5-May	190 (197) 8-June	272 (258) 28-September	174 (186) 22-June	162 10-June
S2	129 (147) 8-May	164 (188) 12-June	209 (240) 27-July	155 (178) 3-June	165 13-June
N1	133 (156) 12-May	173 (183) 21-June	225 (218) 12-August	163 (177) 11-June	174 22-June

The values in parentheses are the corresponding dates (DOY) for xylem

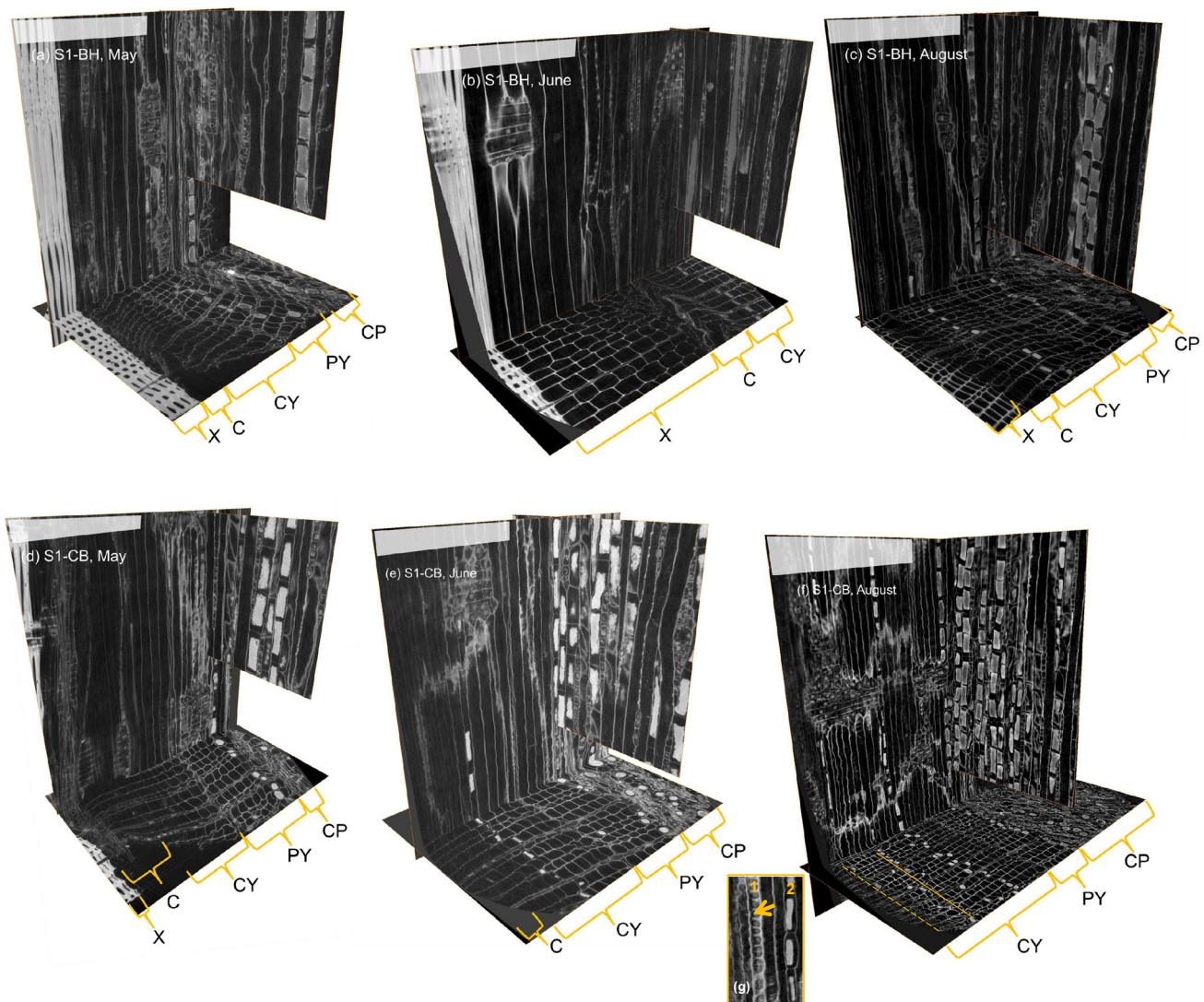


**Fig. 3** Development of Norway spruce phloem during the 2012 growing season in southern Finland (S1-Haapastensyrjä) as visualised in 3D by synchrotron phase-contrast microtomography. Samples were collected in May (**a, d**), June (**b, e**), and August (**c, f**) at breast height (BH; **a, b, c**) and at the base of the living crown (CB; **d, e, f**). The new band of phloem parenchyma was formed by June. A second (marked by a *solid line*) and third layer (marked by a *dashed line*) of

more solitary axial parenchyma was observed at the crown base (**f**). **g** Detail of the sieve pore areas of sieve cell walls (*arrow*); sieve cell wall showing sieve areas is marked by 1, axial parenchyma cells by 2. *X* xylem, *C* cambium, *CY* current-year phloem, *PY* previous-year phloem, *CP* collapsed phloem. Scale bars (in radial direction in  $\mu\text{m}$ ): 250 (**a**), 360 (**b**), 260 (**c**), 330 (**d**), 330 (**e**), 640 (**f**)



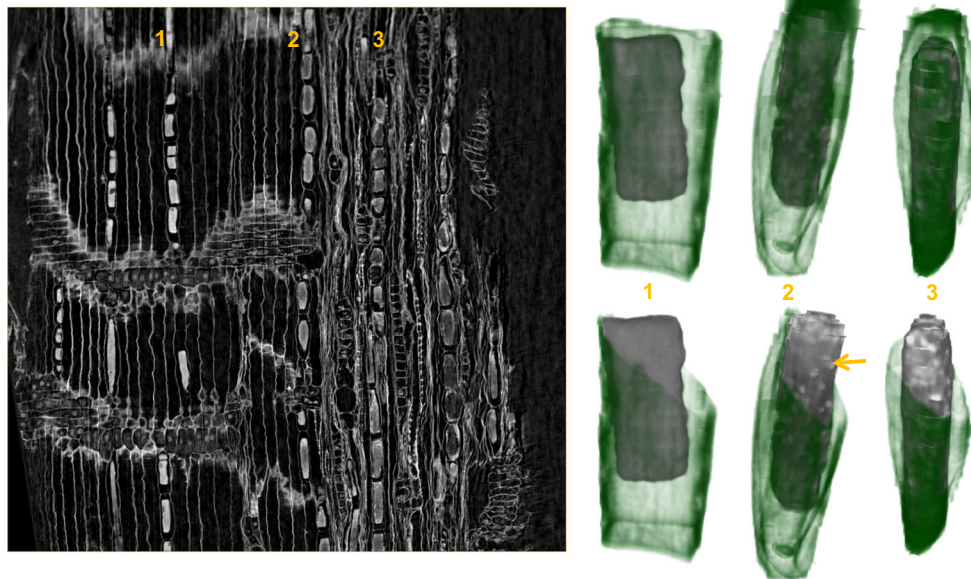


**Fig. 4** On the *left*, Norway spruce phloem (August 2012, S1-Haapastensyrjä, CB) as viewed in radial longitudinal plane, demonstrates the changes in tissue arrangement and cellular features of axial parenchyma from the newest conducting phloem (*left*) towards the outer layers of non-conducting phloem (*right*). On the right, axial parenchyma rendered from the newest (1), previous-year non-collapsed phloem (2), and older collapsed phloem (3) (August

2012, S1-Haapastensyrjä, BH) following the same radial file of sieve cells (i.e. the derivatives of the same cambial initial). Cell walls are rendered in *green*, cell contents in *grey*. Renderings are not to scale; the sizes of the parenchyma in radial, tangential, and axial directions are  $30 \times 39 \times 83 \mu\text{m}^3$  (1),  $40 \times 38 \times 110 \mu\text{m}^3$  (2), and  $32 \times 31 \times 106 \mu\text{m}^3$  (3). The *arrow* indicates starch granules

### Chemical properties of developing phloem

During the most active period of phloem production and differentiation in S1, the amounts of mono- and disaccharides, especially of sucrose, were at their lowest (Figs. 6a, 7a, d). The concentrations of mono- and disaccharides in the newly developing phloem (i.e. the microdissected layer, see Fig. 1) were 6- to 8-fold those of older phloem (i.e. older phloem layers remaining after microdissection; Fig. 6a, b). By July and August (i.e. the time of late phloem formation and active xylem maturation), the amount of sucrose had doubled, whereas the amounts of glucose, fructose, and quinic acid had declined.

At the same time, the amounts of extractives in developing phloem substantially increased (Fig. 6c). Coniferin and sitosterol comprised the majority of the extractives in developing phloem. Notably, after the formation and differentiation of axial parenchyma in June, the amount of stilbene derivatives increased from non-detectable in June to approximately  $1 \mu\text{g mg}^{-1}$  DW in August (Fig. 6c). However, the total amounts of stilbene glucosides and extractives in the older phloem were 117 and 18 times higher, respectively, than in developing tissue (Fig. 6c, d). In the developing tissue, the isorhapontin concentration was twice that of astringin, whereas the older phloem layers contained more astringin than isorhapontin.

During phloem maturation in July, the concentration of non-cellulosic polysaccharides in phloem increased in absolute terms. The relative proportions of different hemicelluloses and pectins within the newest tissue were similar to those in the older phloem, with the exception of the share of glucose: 20 % in new and 40 % in older phloem (Fig. 6e, f).

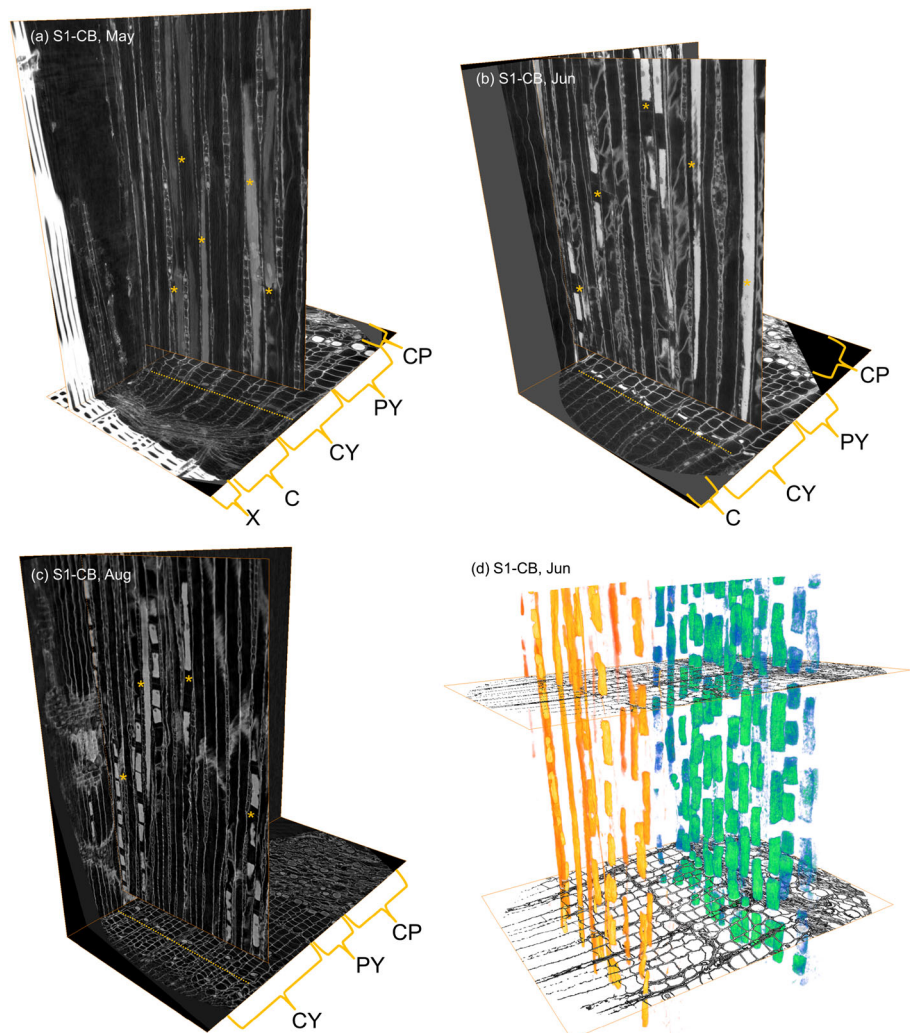
### Variability in NSC content of inner bark

The amounts of NSCs, i.e. starch and soluble sugars, in inner bark showed marked seasonal changes (Table 3; Fig. 7). The differences between sites were generally small and statistically insignificant, except for higher concentrations of sucrose and myo-inositol at the northern site N1, on average over all sampling dates (Table 3).

The starch amount increased significantly from dormant conditions in March to active growth in May and June, when cambial reactivation occurred and the cell division rate peaked (Fig. 7a–c). The starch content then steadily decreased during the second half of the growing season. The total amount of soluble sugars followed the opposite trend: the highest level was found during the rest and dormant periods, and the lowest amount was detected during the time of the highest cambial activity (Fig. 7a–f).

The amount of sucrose reached its maximum at the time of late phloem formation in August in southern Finland (S1

**Fig. 5** Differentiation of axial parenchyma in Norway spruce phloem during the 2012 growing season in southern Finland (S1-Haapastensyrjä, CB). The tangential cross-sections have as closely as possible aligned with the current-year row of developing parenchyma (*dashed line* in the axial cross-section). At the beginning of the growing season (a) most of the parenchyma still lack discernible transverse walls in the imaged volume (height approx. 0.7 mm). The transverse walls are then developed later (b–c), along with the accumulation of phenolic stilbene glucosides in the axial parenchyma, which could also be seen as the cellular contents becoming brighter in the tomography images. 3D renderings (d) highlight the difference in cell length between the current (*orange/red*) and previous-year (*blue/green*) axial parenchyma in the June sample. Asterisks denote axial parenchyma. The size of the volume shown in radial, tangential and axial directions is  $658 \times 439 \times 704 \mu\text{m}^3$  (a),  $663 \times 530 \times 704 \mu\text{m}^3$  (b), and  $1280 \times 664 \times 1246 \mu\text{m}^3$  (c)



and S2) and in July at the northern site (N1). At the same time, the carbon demand in xylem was probably high due to secondary cell wall deposition (Fig. 3c). Hexoses (i.e. glucose and fructose) had the lowest concentrations during active secondary growth and showed increased levels during the dormant season. Similarly, raffinose and stachyose tended to have significantly higher concentrations during dormancy than during the growing period. The concentrations of pinitol, sorbitol, and myo-inositol were low and showed no clear seasonal variability (Fig. 7d–f).

### Variability in stilbene glucoside content of inner bark

The amounts of stilbene glucosides in inner bark varied significantly between the sampling dates at the northern site, N1 (Table 3; Fig. 7g–i), but no significant site  $\times$  period interaction was found. In the samples from

mid-summer to autumn and winter, the concentrations of total stilbene glucosides, piceid, and astringin significantly increased over those from spring and early summer, especially in samples from the northernmost site (N1). The initial increase in stilbene glucoside level coincided with the time when new band(s) of axial parenchyma were formed and cells differentiated, the rate of cambial divisions was slowing, secondary walls in xylem were actively being built, and the amount of soluble sugars (especially of sucrose) in inner bark was high. The trees at the northern site (N1) had increased levels of isorhapontin, and as a result, they contained higher total amounts of stilbene glucosides than did the trees from southern Finland (S1, S2). The seasonal pattern of total stilbene glucoside content of inner bark was significantly correlated with seasonal changes in the amounts of glucose, fructose, and raffinose (Fig. 8). In contrast, the total stilbene glucoside amount was not correlated with the amounts of

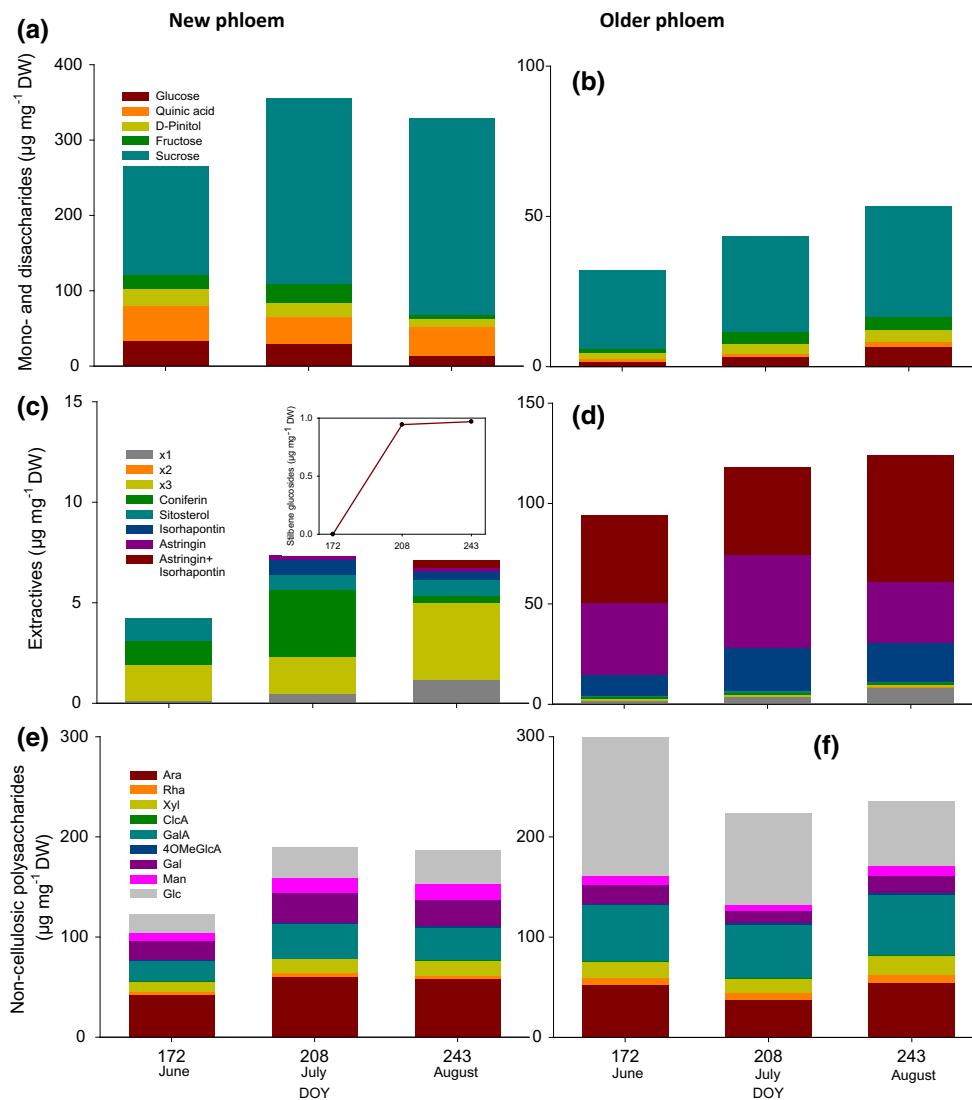


**Fig. 6** Chemical properties of laser-microdissected developing phloem ring (a, c, e) and remaining older phloem (b, d, f) layers of Norway spruce during the 2012 growing season in southern Finland (S1-Haapastensyrjä): the content of mono- and disaccharides (a, b), extracts (c, d), and non-cellulosic polysaccharides (e, f). A small

graph (c) indicates the change of the total stilbene glucosides. c, d x1–x3, unidentified extracts. e, f Ara arabinose, Rha rhamnose, Xyl xylose, GlcA glucuronic acid, GalA galacturonic acid, 4OMeGlcA 4-O-methyl-glucuronic acid, Gal galactose, Man mannose, Glc glucose

other studied soluble sugars or starch ( $P > 0.05$ ; data not shown).

**Discussion**

To gain new insights into the coordination of phloem formation in mature *Picea abies* stems, we monitored within-year phloem cell production and seasonal variation in the amounts of primary and secondary metabolites, visualised phloem development in 3D, and measured the chemical properties of the newest phloem tissues isolated by laser microdissection. In particular, we studied the development

of axial phloem parenchyma that contributes to phloem storage and defence.

**Phloem production and structural development**

From 10 to 15 new cells in a radial file of the phloem growth ring were produced during the 2012 growing season. In all the study trees, the seasonal pattern of phloem formation was similar. As the functional life of sieve elements is strikingly short compared with that of xylem tracheids, only 1 to 2 years (Evert 2006), a tree needs to continually invest carbon in building new phloem in order to survive. In our study, the onset of phloem cell

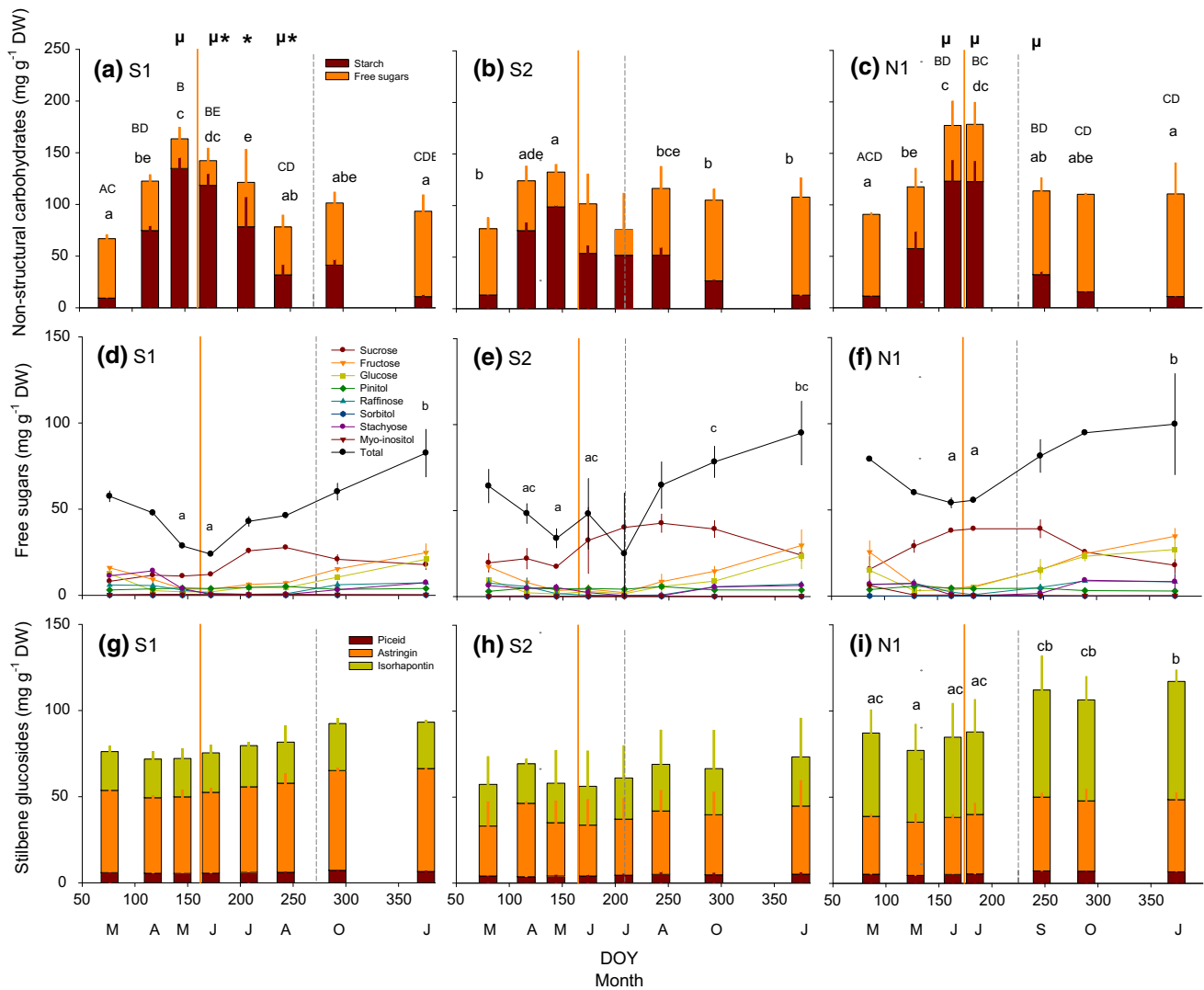


**Fig. 7** Seasonal variation in the amounts of primary and secondary metabolites of inner bark in Norway spruce in southern Finland (**a, d, g**, S1-Haapastensyrjä; **b, e, h**, S2-Ruotsinkylä) and northern Finland (**c, f, i**, N1-Kivalo): total non-structural carbohydrates (i.e. the sum of soluble sugars and starch, **a, b, c**), different soluble sugars (**d, e, f**), and phenolic stilbene glucosides (**g, h, i**) ( $\pm$ SD). Different *uppercase*

*letters* indicate statistically significant differences in the total amount of NSC (**a, b, c**), and different *lowercase letters* indicate significant differences in starch (**a, b, c**), free sugar (**d, e, f**), and the amount of stilbene glucoside (**g, h, i**) between sampling periods at each site. The *vertical lines* are the same as in Fig. 2. Asterisk sample for chemical microanalysis;  $\mu$ , sample for  $\mu$ CT of developing phloem (see Table 1)

production occurred in early to mid-May, about 3 weeks before the onset of xylem cell production. The observed timing agrees with previous results on within-year xylem formation of Norway spruce in Finland. About 5 % of the annual tracheid production has usually been produced by late May in the south and by mid-June in the north part of the country (Mäkinen et al. 2003; Henttonen et al. 2009; Jyske et al. 2014a).

In boreal and temperate conditions, the timing and rate of secondary growth, especially the onset of growth, is typically controlled by temperature (Begum et al. 2013), while photoperiod may play a role in growth cessation in the fall (Rossi et al. 2006b). In our study, other critical

phenological dates of phloem formation, including the date of maximal cell production, also preceded those of xylem. Previous research has likewise shown that the phloem and xylem formation phases are not synchronised (Gričar et al. 2014). In the temperate region, for instance, the highest rate of phloem cell production of Norway spruce was detected 2–6 weeks earlier than that of xylem (Gričar et al. 2014). We found that a few phloem derivatives remained in undifferentiated stage during late autumn and winter. In the secondary phloem of *Pinus resinosa*, *P. banksiana*, and *P. strobus*, the 2–4 sieve cells that formed last have been reported to stay alive over the winter (Alfieri and Evert 1968).

**Table 3** Tests (*F* and *P* values) of the contribution of site and sampling period to the amounts of primary and secondary metabolites of inner bark during the 2012 growing season

Variable	Site		Period		Site × period	
	<i>F</i>	<i>P</i>	<i>F</i>	<i>P</i>	<i>F</i>	<i>P</i>
Non-structural carbohydrates (NSCs)						
Total NSCs (soluble sugars + starch)	3.88	0.147	14.37	<0.0001	2.36	0.037
Starch	4.2	0.135	72.83	<0.0001	5.18	<0.001
Total soluble sugars	7.69	0.066	12.7	<0.0001	0.68	0.767
Sucrose	16.71	0.024	12.74	<0.0001	2.76	0.018
Glucose	3.49	0.165	32.08	<0.0001	1.93	0.084
Fructose	1.54	0.346	49.71	<0.0001	2.58	0.024
Raffinose	1.57	0.342	12.12	<0.0001	0.72	0.736
Stachyose	5.34	0.103	59.14	<0.0001	10.11	<0.0001
Pinitol	0.12	0.887	6.53	<0.001	1.08	0.426
Myo-inositol	9.85	0.048	35.56	<0.0001	41.02	<0.0001
Sorbitol	0.06	0.946	11.28	<0.0001	2.76	0.018
Stilbene glucosides						
Total stilbenes	14.98	0.028	10.03	<0.0001	1.84	0.099
Piceid	3.18	0.182	4.94	0.002	1.06	0.439
Astringin	2.13	0.266	7.7	<0.001	1.95	0.081
Isorhapontin	10.97	0.042	1.97	0.109	1.14	0.382

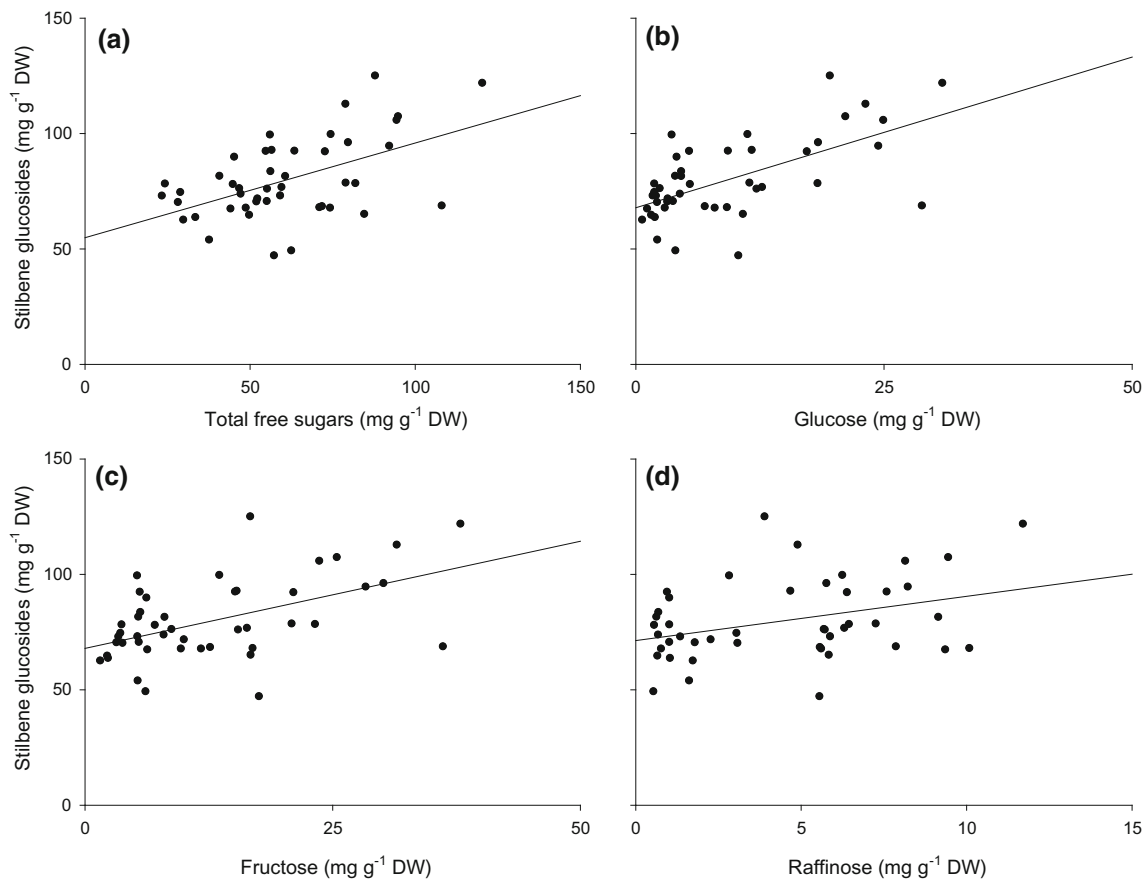


**Fig. 8** Pearson correlations between the contents of non-structural carbohydrates (a total soluble sugars; b glucose; c fructose; d raffinose) and total amount of phenolic stilbene glucosides of the inner

bark in Norway spruce. Data from all sites and sampling periods were pooled (*n* = 6 trees)

Compared with xylem, phloem shows less variability in its within-year dynamics of formation and annual cell number (Gričar and Čufar 2008; Prislán et al. 2013). Phloem is assumed to be less affected by environmental factors and more tightly controlled by intrinsic factors than xylem (Alfieri and Evert 1968; Gričar et al. 2014). Nevertheless, the overwintering phloem derivatives in our study trees rapidly responded to increasing air temperatures during early spring, re-initiating their maturation processes.

Our 3D analysis of phloem revealed a flattening of older sieve cells and the replacement of these cells by new ones, especially towards the end of the growing period. The imaging also revealed the special features of developing phloem and xylem: cell wall thickening, development of sieve pore areas (Fig. 3g), and changes in the size and appearance of developing axial phloem parenchyma.  $\mu$ Ct analysis revealed that the differentiation of axial parenchyma was initiated in late May by the development of elongated cells with shape and length similar to those of sieve cells. The differentiation was continued by transverse divisions of the cells and the development of transverse walls by June, as well as by the increase in cellular contents and changes in cell shape by August. Our findings support the findings of Krekling et al. (2000), who also discovered that the differentiation of axial parenchyma is longer process than that of sieve cells and can continue for several years.

The seasonal fluctuations of starch granule accumulation from axial and ray parenchyma were visible as well. Moreover, 3D imaging clearly visualised tissue-level changes across bark from cambium to older phloem layers, such as dilatation of rays and secondary changes in axial parenchyma. Microtomography obviously offers many advantages over traditional light microscopic approaches in studying the structures and networks of vascular tissues, as it produces high-throughput data from significantly larger tissue volumes.

### Interrelations of phloem formation and seasonal variation in NSCs

At all three study sites, the timing of early phloem production and the maximal rate of phloem cell production were coupled with the highest seasonal amounts of total NSC (due to the high starch amounts) in inner bark. In our study and that by Gruber et al. (2013) on *Pinus cembra*, the starch content in inner bark significantly increased from winter towards late spring and mid-summer, then decreased again towards autumn and winter. The soluble sugars, in contrast, decreased from a high concentration during the dormant season to their lowest level during active growth, then again increased towards the end of the growing period. The strong seasonal cycle followed by NSC and starch is

well documented in several species and geographical locations: the resynthesis of starch in early spring and its breakdown for resistance to freezing during the cold season in stems, needles, and the cambial zone (Kozłowski 1992; Simard et al. 2013). The amount of starch in cambium and trunk wood has been shown to deplete during cambial reactivation and increase again by the time of xylem differentiation (Begum et al. 2010, 2013). Budburst, cambial reactivation, and early phloem formation appear to rely primarily on stored carbon, whereas new photoassimilates are more abundantly available by the time of xylem formation and differentiation (Oribe et al. 2003; Begum et al. 2013). In our study, sucrose levels increased in early spring and reached their maximum after mid-summer (i.e. after the early phloem formation had completed), thus allowing late phloem formation, secondary-wall thickening in xylem, and accumulation of extractives in the newest phloem ring to coincide. In a previous study of Siberian larch, the carbohydrate content considerably increased in the newest phloem after cellular maturation (Antonova and Stasova 2008). In our study, coniferin (coniferyl alcohol glucoside) was the most abundant extractive in the newest phloem in June and July. This glycosylated monolignol is assumed to be a transport and storage form of a precursor in lignification (Liu et al. 2011; Tsuyama et al. 2013) and has been found in the cambial sap of several species (Whetten et al. 1998).

Our results on phloem formation and NSCs mainly confirmed the hypothesis: a clear temporal coupling existed between the resumption and progress of phloem cell production and seasonal variation in NSCs. The results suggest that phloem formation was not restricted by the availability of carbohydrates, but responded merely to environmental constraints on sink activity (Sundberg et al. 1993), as has been proposed for timberline species (Hoch et al. 2002; Gruber et al. 2013; Simard et al. 2013). Nevertheless, all the seeming excess of NSCs (especially starch) in inner bark during the onset and maximal rate of phloem production may not have served as substrates for secondary growth. Instead, part of the NSC might have been transported to other sinks, sequestered, or even actively stored in long-term pools, possibly providing a buffer during severe stress periods (McDowell et al. 2008; Sala et al. 2012; Martínez-Vilalta 2014; Sevanto et al. 2014).

### Relationship between phloem formation and seasonal variation in stilbene glucosides

Stilbenic compounds are derived from the phenylalanine/polymalonate pathway, in which stilbene synthase catalyses the last steps of biosynthesis. In Norway spruce, resveratrol (i.e. aglycon of piceid) is apparently an intermediary that undergoes modifications (hydroxylation,

methoxylation, and glycosylation) to yield astringin and isorhapontin (Hammerbacher et al. 2011). Our results support earlier findings that the axial phloem parenchyma is the main site of phenolic stilbene glucoside accumulation in Norway spruce phloem (Li et al. 2012). The first axial parenchyma band formed by mid-June, coinciding with the culmination of the period of the fastest phloem cell production. The axial parenchyma appeared first as elongated cells (detected in late May), and their differentiation included transverse divisions and the development of transverse walls, which we detected by  $\mu$ CT (from the samples collected in late June). The differentiation of axial parenchyma was followed by the accumulation of astringin and isorhapontin in the newest phloem tissue. At the same time, axial parenchyma enlarged and 3D imaging showed that cell contents were becoming larger and denser. Thus, the results confirmed our hypothesis that temporal and developmental relationships existed between axial phloem parenchyma formation and the accumulation of phenolic stilbene glucosides.

Related to this, seasonal and developmental changes in the appearance of phenolic inclusions inside axial parenchyma cells (i.e. polyphenolic parenchyma) have been visualised (Krekling et al. 2000; Franceschi et al. 2005). The staining density of phenolic bodies (osmium tetroxide and Stevel's blue stains in electron and optical microscopy, respectively) decreased during spring and increased during autumn and winter in all the axial parenchyma cells of 25-year-old Norway spruce growing in Norway (Krekling et al. 2000). Thus, the phenolic deposits of axial parenchyma cells may not be stable structures (Toscano Underwood and Pearce 1991a; Franceschi et al. 2005).

In earlier investigations, increasing amounts of stilbene glucosides were also detected in spruce bark during summer and early autumn (Solhaug 1990). We detected slightly increasing amounts of stilbene glucosides in inner bark during the period from mid-summer to the dormant period. This increase was significantly coupled with increasing levels of hexoses (glucose and fructose) and raffinose, which are generally known as freeze-resistant sugars that alleviate the cold-induced stress in living cells (Nishizawa et al. 2008). The increases in the amounts of stilbene glucoside as the dormant period approached raises questions about their possible protective role in freezing stress, e.g. scavenging the radical oxygen species that accumulate in the cold (Kendall and McKersie 1989; Baek and Skinner 2012). The slightly higher amounts of stilbene glucoside that we detected in the inner bark of trees from the northernmost site (N1) compared with those from the southern sites (S1 and S2) represent a possible adaptation to harsher environmental conditions in the trees growing in the colder environment. The observed correlations between stilbene glucosides and sugars might simply be explained by the

increasing availability of substrates for stilbene biosynthesis and glycosylation. The overall amount of stilbene glucosides found in this study was in accordance with earlier findings: the inner bark of spruce typically contains 5–10 % stilbene glucosides (Woodward and Pearce 1988; Toscano Underwood and Pearce 1991a, b; Krogell et al. 2012; Latva-Mäenpää et al. 2013, 2014; Jyske et al. 2014b).

Our results indicate that stilbene biosynthesis occurs concurrently in the newest developing phloem and the older phloem layers after the formation and differentiation of new axial parenchyma. As high carbon demands in the developing xylem occur simultaneously, due to the need to build up lignified secondary walls, a tree invests carbon simultaneously in secondary growth and defence-related extractives. In a related study, *Populus trichocarpa* seedlings were recently shown by  $^{13}\text{C}$  pulse-labelling to allocate carbon to defensive phenolic glucosides (salicoids) in expanding leaves throughout the growing season (Massad et al. 2014). The study determined that *P. trichocarpa* followed an optimal defence strategy, as it invested newly assimilated carbon into secondary metabolites directly after labelling. Further labelling experiments would shed more light on carbon allocation strategies in various species, as well as the possible turnover metabolism of stilbene glucosides in Norway spruce.

## Conclusions

In this study, our integrative approach revealed how within-year phloem cell production of mature Norway spruce trees in a boreal region (northern and southern Finland) was associated with seasonal changes in NSC pools and secondary phenolic metabolites (i.e. stilbene glucosides) of inner bark. We also recorded for the first time the quantitative changes in the amounts of mono- and disaccharides, extractives, and non-cellulosic polysaccharides of developing phloem tissues isolated by laser microdissection during a growing season. At the same time, we showed that the modifications in chemical properties were interlinked with developmental changes in axial phloem parenchyma at the tissue, cellular, and sub-cellular level as visualised in 3D, that is, through the formation of a tangential band, the transverse divisions and differentiation of cells, and finally enlargement of cell size and cell contents. Our results indicate that the complementary use of novel microtechniques can provide new perspectives on understanding the formation, structure, and chemistry of phloem in trees.

*Author contribution statement* TJ designed and performed the research, analysed the results, carried out the statistical testing, and wrote the article. J-PS performed the  $\mu$ CT measurements and analysis. AP performed the

chemical microanalysis. TL carried out NSC analysis. UW provided facilities and help for laser microdissection. KK and HA helped design and implement the study. All authors read and approved the manuscript.

**Acknowledgments** We thank the staff of the Finnish Forest Research Institute, and several students and trainees, for assisting in field and laboratory work. We also thank Dr. P. Saranpää, Dr. H. Mäkinen, and Prof. B. Holmbom for their help designing of the study. We are grateful to the Electron Microscopy Unit of the Institute of Biotechnology, University of Helsinki, for providing laboratory facilities and help in sample preparation. We acknowledge the European Synchrotron Radiation Facility (ESRF) for providing beam time for the  $\mu$ CT measurements, and are grateful for P. Tafforeau and C. Soriano for their help in using beamline ID19. P. Ahvenainen, A. Kallonen, A. Meaney, and K. Pirkkalainen of the Department of Physics, University of Helsinki, provided valuable assistance in carrying out the  $\mu$ CT experiments. Prof. R. Serimaa is acknowledged for her help designing the study and participating in the  $\mu$ CT experiment. This study was carried out under the framework of the COST FP1106 network STReESS and funded by the post-doctoral research grant from the Academy of Finland (no. 250299). This work was also supported by JSPS KAKENHI Grant No. 26-04395 and JSPS post-doctoral Grant No. P14395.

## References

- Alfieri FJ, Evert RF (1968) Seasonal development of the secondary phloem in *Pinus*. *Am J Bot* 55:518–528
- Antonova GF, Stasova VV (2006) Seasonal development of phloem in scots pine stems. *Ontogenez* 37:368–382
- Antonova GF, Stasova VV (2008) Seasonal development of phloem in Siberian larch stems. *Russ J Dev Biol* 39:207–218
- Baek K-H, Skinner DZ (2012) Production of reactive oxygen species by freezing stress and the protective roles of antioxidant enzymes in plants. *J Agric Chem Environ* 1:34–40
- Begum S, Nakaba S, Oribe Y, Kubo T, Funada R (2010) Changes in the localization and levels of starch and lipids in cambium and phloem during cambial reactivation by artificial heating of main stems of *Cryptomeria japonica* trees. *Ann Bot* 106:885–895
- Begum S, Nakaba S, Yamagishi Y, Oribe Y, Funada R (2013) Regulation of cambial activity in relation to environmental conditions: understanding the role of temperature in wood formation of trees. *Physiol Plant* 147:46–54
- Brodersen CR (2013) Visualizing wood anatomy in three dimensions with high-resolution X-ray microtomography (MCT)—a review. *IAWA J* 34:408–424
- Chong J, Poutaraud J, Huguency P (2009) Metabolism and roles of stilbenes in plants. *Plant Sci* 177:143–155
- Cochard H, Delzon S, Badel E (2015) X-ray microtomography (micro-CT): a reference technology for high-resolution quantification of xylem embolism in trees. *Plant Cell Environ* 38:201–206
- Deslauriers A, Giovannelli A, Rossi S, Castro G, Fragnelli G, Traversi L (2009) Intra-annual cambial activity and carbon availability in stem of poplar. *Tree Physiol* 29:1223–1235
- Deslauriers A, Beaulieu M, Balducci L, Giovannelli A, Gagnon MJ, Rossi S (2014) Impact of warming and drought on carbon balance related to wood formation in black spruce. *Ann Bot* 114:335–345
- Evert RF (2006) *Esau's plant anatomy. Meristems, cells, and tissues of the plant body: their structure, function, and development.* Wiley, Hoboken
- Franceschi V, Krekling T, Berryman A, Christiansen E (1998) Specialized phloem parenchyma cells in Norway spruce (*Pinaceae*) bark are an important site of defense reactions. *Am J Bot* 85:601–615
- Franceschi VR, Krokene P, Krekling T, Christiansen E (2000) Phloem parenchyma cells are involved in local and distant defense responses to fungal inoculation or bark-beetle attack in Norway spruce (*Pinaceae*). *Am J Bot* 87:314–326
- Franceschi VR, Krokene P, Christiansen E, Krekling T (2005) Anatomical and chemical defenses of conifer bark against bark beetles and other pests. *New Phytol* 167:353–375
- Froelich DR, Mullendore DL, Jensen KH, Ross-Elliott TJ, Anstead JA, Thompson GA, Pélissier HC, Knoblauch M (2011) Phloem ultrastructure and pressure flow: sieve-element-occlusion-related agglomerations do not affect translocation. *Plant Cell* 23:4428–4445
- Giovannelli A, Emiliani G, Traversi ML, Deslauriers A, Rossi S (2011) Sampling cambial region and mature xylem for non structural carbohydrates and starch analyses. *Dendrochronologia* 29:177–182
- Gričar J, Čufar K (2008) Seasonal dynamics of phloem and xylem formation in silver fir and Norway spruce as affected by drought. *Russ J Plant Physiol* 55:538–543
- Gričar J, Prislán P, Gryc V, Vavřík H, de Luis M, Čufar K (2014) Plastic and locally adapted phenology in cambial seasonality and production of xylem and phloem cells in *Picea abies* from temperate environments. *Tree Physiol* 34:869–881. doi:10.1093/treephys/tpu026
- Gruber A, Pirkebner D, Oberhuber W (2013) Seasonal dynamics of mobile carbohydrate pools in phloem and xylem of two alpine timberline conifers. *Tree Physiol* 33:1076–1083
- Hammerbacher A, Ralph SG, Bohlmann J, Fenning TM, Gershenzon J, Schmidt A (2011) Biosynthesis of the major tetrahydroxystilbenes in spruce, astringin and isorhapontin, proceeds via resveratrol and is enhanced by fungal infection. *Plant Physiol* 157:876–890
- Henttonen HM, Mäkinen H, Nöjd P (2009) Seasonal dynamics of the radial increment of Scots pine and Norway spruce in the southern and middle boreal zones in Finland. *Can J For Res* 39:606–618
- Herms DA, Mattson WJ (1992) The dilemma of plants: to grow or defend. *Quart Rev Biol* 67:283–335
- Hoch G, Popp M, Korner C (2002) Altitudinal increase of mobile carbon pools in *Pinus cembra* suggests sink limitation of growth at the Swiss treeline. *Oikos* 98:361–374
- Jyske T, Hölttä T (2015) Comparison of phloem and xylem hydraulic architecture in *Picea abies* stems. *New Phytol* 205:102–115
- Jyske T, Mäkinen H, Kalliokoski T, Nöjd P (2014a) Intra-annual tracheid production of Norway spruce and Scots pine across a latitudinal gradient in Finland. *Agr For Meteorol* 194:241–254
- Jyske T, Laakso T, Latva-Mäenpää H, Tapanila T, Saranpää P (2014b) Yield of stilbene glucosides from the bark of young and old Norway spruce stems. *Biomass Bioenergy* 71:216–227
- Kendall EJ, McKersie BD (1989) Free radical and freezing injury to cell membranes of winter wheat. *Physiol Plant* 76:86–94
- Kozłowski TT (1992) Carbohydrate sources and sinks in woody plants. *Bot Rev* 58:107–222
- Krekling T, Franceschi VR, Berryman AA, Christiansen E (2000) The structure and development of polyphenolic parenchyma cells in Norway spruce (*Picea abies*) bark. *Flora* 195:354–369
- Krogell J, Holmbom B, Pranovich A, Hemming J, Willför S (2012) Extraction and chemical characterization of Norway spruce inner and outer bark. *Nord Pulp Pap Res J* 27:6–17
- Krokene P, Nagy NE, Solheim H (2008) Methyl jasmonate and oxalic acid treatment of Norway spruce: anatomically based defense



- responses and increased resistance against fungal infection. *Tree Physiol* 28:29–35
- Larson PR (1994) The vascular cambium: development and structure. Springer, Berlin
- Latva-Mäenpää H, Laakso T, Sarjala T, Wähälä K, Saranpää P (2014) Root neck of Norway spruce as a source of bioactive lignans and stilbenes. *Holzforschung* 68:1–7
- Latva-Mäenpää H, Laakso T, Sarjala T, Wähälä K, Saranpää P (2013) Variation of stilbene glucosides in bark extracts obtained from roots and stumps of Norway spruce (*Picea abies* [L.] Karst.). *Trees* 27:131–139
- Leroux O, Leroux F, Bellefroid E, Claeys M, Couvreur M, Borgonie G, Van Hoorebeke L, Masschaele B, Viane R (2009) A new preparation method to study fresh plant structures with X-ray computed tomography. *J Microsc* 233:1–4
- Li SH, Nagy NE, Hammerbacher A, Krokene P, Niu XU, Gershenzon J et al (2012) Localization of phenolics in phloem parenchyma cells of Norway spruce (*Picea abies*). *Chem Bio Chem* 13:2707–2713
- Liu J-L, Miao Y-C, Zhang K-W (2011) Sequestration and transport of lignin monomeric precursors. *Molecules* 16:710–727
- Mäkinen H, Nöjd P, Saranpää P (2003) Seasonal changes in stem radius and production of new tracheids in Norway spruce. *Tree Physiol* 23:959–968
- Manach C, Scalbert A, Morand C, Rémésy C, Jiménez L (2004) Polyphenols: food sources and bioavailability. *Am J Clin Nutr* 79:727–747
- Martínez-Vilalta J (2014) Carbon storage in trees: pathogens have their say. *Tree Physiol* 34:215–217. doi:10.1093/treephys/tpu010
- Massad T, Trumbore SE, Ganbat G, Reichelt M, Unsicker S, Boeckler A, Gleixner G, Gershenzon J, Ruehlow S (2014) An optimal defense strategy for phenolic glycoside production in *Populus trichocarpa* – isotope labeling demonstrates secondary metabolite production in growing leaves. *New Phytol* 203:607–619. doi:10.1111/nph.12811
- McDowell NG, Pockman W, Allen C et al (2008) Mechanisms of plant survival and mortality during drought: why do some plants survive while others succumb? *New Phytol* 178:719–739
- Nagy NE, Franceschi VR, Solheim H, Krekling T, Christiansen E (2000) Wound-induced traumatic resin duct development in stems of Norway spruce (Pinaceae): anatomy and cytochemical traits. *Am J Bot* 87:302–313
- Nishizawa A, Yabuta Y, Shigeoka S (2008) Galactinol and raffinose constitute a novel function to protect plants from oxidative damage. *Plant Physiol* 147:1251–1263
- Oribe Y, Funada R, Kubo T (2003) Relationships between cambial activity, cell differentiation and the localization of starch in storage tissues around the cambium in locally heated stems of *Abies sachalinensis* (Schmidt) Masters. *Trees* 17:185–192
- Prislan P, Gričar J, de Luis M, Smith KT, Čufar K (2013) Phenological variation in xylem and phloem formation in *Fagus sylvatica* from two contrasting sites. *Agric For Meteorol* 180:142–151
- Robb EL, Stuart JA (2014) The stilbenes resveratrol, pterostilbene and piceid affect growth and stress resistance in mammalian cells via a mechanism requiring estrogen receptor beta and the induction of Mn-superoxide dismutase. *Phytochemistry* 98:164–173
- Rossi S, Deslauriers A, Morin H (2003) Application of the Gompertz equation for the study of xylem cell development. *Dendrochronologia* 21:33–39
- Rossi S, Anfodillo T, Menardi R (2006a) Trephor: a new tool for sampling microcores from tree stems. *IAWA J* 27:89–97
- Rossi S, Deslauriers A, Anfodillo T, Morin H, Saracino A, Motta R, Borghetti M (2006b) Conifers in cold environments synchronize maximum growth rate of tree-ring formation with day length. *New Phytol* 170:301–310
- Rossi M, Caruso F, Antonioletti R, Viglianti A, Traversi G, Leone S, Basso E, Cozzi R (2013) Scavenging of hydroxyl radical by resveratrol and related natural stilbenes after hydrogen peroxide attack on DNA. *Chem Biol Interact* 206:175–185
- Ryan MG, Asao S (2014) Phloem transport in trees. *Tree Physiol* 34:1–4
- Sala A, Woodruff DR, Meinzer FC (2012) Carbon dynamics in trees: feast or famine? *Tree Physiol* 32:764–775
- Sevanto S, McDowell NG, Dickman LT, Pangle R, Pockman WT (2014) How do trees die? A test of the hydraulic failure and carbon starvation hypotheses. *Plant Cell Environ* 37:153–161
- Simard S, Giovannelli A, Treydte K, Traversi ML, King GM, Frank D, Fonti P (2013) Intra-annual dynamics of non-structural carbohydrates in the cambium of mature conifer trees reflects radial growth demands. *Tree Physiol* 33:913–923
- Solhaug K (1990) Stilbene glucosides in bark and needles from *Picea* species. *Scand J For Res* 5:59–67
- Spicer R (2014) Symplasmic networks in secondary vascular tissues: parenchyma distribution and activity supporting long-distance transport. *J Exp Bot* 65:1829–1848
- Sundberg B, Ericsson A, Little CHA, Nasholm T, Gref R (1993) The relationship between crown size and ring width in *Pinus sylvestris* L. stems: dependence on indole-3-acetic acid, carbohydrates and nitrogen in the cambial region. *Tree Physiol* 12:347–362
- Sundberg A, Sundberg K, Lillandt C, Holmbom B (1996) Determination of hemicelluloses and pectins in wood and pulp fibres by acid methanolysis and gas chromatography. *Nord Pulp Paper Res J* 11(216–219):226
- Toscano Underwood CD, Pearce RB (1991a) Astringin and isorhapontin distribution in Sitka spruce trees. *Phytochemistry* 30:2183–2218
- Toscano Underwood CD, Pearce RB (1991b) Variation in the levels of the antifungal stilbene glucosides astringin and isorhapontin in the bark of Sitka spruce (*Picea sitchensis* (Bong.) Carr.). *Eur J For Pathol* 21:279–289
- Trockenbrodt M (1990) Survey and discussion of the terminology used in bark anatomy. *IAWA Bull* 11:141–166
- Truernit E (2014) Phloem imaging. *J Exp Bot* 65:1681–1688
- Tsuyama T, Kawai R, Shitan N, Matoh T, Sugiyama J, Yoshinaga A, Takabe K, Fujita M, Yazaki K (2013) Proton-dependent coniferin transport, a common major transport event in differentiating xylem tissue of woody plants. *Plant Physiol* 162:918–926
- van Bel AJE (1990) Xylem-phloem exchange via the rays: the undervalued route of transport. *J Exp Bot* 41:631–644
- van Bel AJE (2003) The phloem, a miracle of ingenuity. *Plant Cell Environ* 26:125–149
- Whetten RW, MacKay JJ, Sederoff RR (1998) Recent advances in understanding lignin biosynthesis. *Annu Rev Plant Physiol Plant Mol Biol* 49:585–609
- Witzell J, Martin J (2008) Phenolic metabolites on the resistance of northern forest trees to pathogens: past experiences and future prospects. *Can J For Res* 38:2711–2727
- Woodward S, Pearce RB (1988) The role of stilbenes in resistance of Sitka spruce (*Picea sitchensis* (Bong.) Carr.) to entry of fungal pathogens. *Physiol Mol Plant Pathol* 33:127–149
- Zeide B (1993) Analysis of growth equations. *For Sci* 39:594–616